Journal of Neuroscience Methods 268 (2016) 87–97

Contents lists available at ScienceDirect

Journal of Neuroscience Methods

journal homepage: www.elsevier.com/locate/jneumeth

Non-parametric directionality analysis – Extension for removal of a single common predictor and application to time series

David M. Halliday[a,*], Mohd Harizal Senik[b], Carl W. Stevenson[c], Rob Mason[b]

[a] Department of Electronics, University of York, York YO10 5DD, UK
[b] School of Life Sciences, University of Nottingham, Nottingham NG7 2UH, UK
[c] School of Biosciences, University of Nottingham, Loughborough LE12 5RD, UK

HIGHLIGHTS

- We describe non-parametric estimates of conditional directionality between signals.
- Scalar metrics decompose the conditional product moment correlation by direction.
- Additional functions decompose the partial coherence estimate by direction.
- Method is applied to simulated (cortical neuron) and real (hippocampal LFP) data.
- Framework can be applied to time series and spike train data.

ARTICLE INFO

Article history:
Received 16 December 2015
Received in revised form 18 March 2016
Accepted 4 May 2016
Available online 7 May 2016

Keywords:
Directionality
Partial coherence
Non-parametric
Time series
Point process
Conditional independence
Granger causality

ABSTRACT

Background: The ability to infer network structure from multivariate neuronal signals is central to computational neuroscience. Directed network analyses typically use parametric approaches based on auto-regressive (AR) models, where networks are constructed from estimates of AR model parameters. However, the validity of using low order AR models for neurophysiological signals has been questioned. A recent article introduced a non-parametric approach to estimate directionality in bivariate data, non-parametric approaches are free from concerns over model validity.
New method: We extend the non-parametric framework to include measures of directed conditional independence, using scalar measures that decompose the overall partial correlation coefficient summatively by direction, and a set of functions that decompose the partial coherence summatively by direction. A time domain partial correlation function allows both time and frequency views of the data to be constructed. The conditional independence estimates are conditioned on a single predictor.
Results: The framework is applied to simulated cortical neuron networks and mixtures of Gaussian time series data with known interactions. It is applied to experimental data consisting of local field potential recordings from bilateral hippocampus in anaesthetised rats.
Comparison with existing method(s): The framework offers a non-parametric approach to estimation of directed interactions in multivariate neuronal recordings, and increased flexibility in dealing with both spike train and time series data.
Conclusions: The framework offers a novel alternative non-parametric approach to estimate directed interactions in multivariate neuronal recordings, and is applicable to spike train and time series data.

1. Introduction

Directed network analyses are widely used in neuroscience to infer network structure in multivariate neural recordings (Rubinov and Sporns, 2010). The majority of approaches are parametric, which rely on estimating the parameters of a model to describe the patten of interactions between the observed signals, typically using auto-regressive (AR) models (Granger, 1969; Geweke, 1982). Once the AR parameters have been estimated different metrics relating to directionality can be constructed directly as a function of the model parameters (Baccala and Sameshima, 2001; Kaminski et al., 2001; Chen et al., 2006; Schelter et al., 2006; Chicharro, 2012). A number of concerns have been raised regarding the validity of AR models to accurately capture the complex structure present

* Corresponding author.
E-mail address: david.halliday@york.ac.uk (D.M. Halliday).

http://dx.doi.org/10.1016/j.jneumeth.2016.05.008
0165-0270/

in multivariate neural and other time series typically encountered in scientific problems (Gersch, 1972; Thomson and Chave, 1991; Lindsay and Rosenberg, 2011). A number of alternative non-parametric approaches have been considered to describe directed interactions in neurophysiological signals (Gersch, 1972; Eichler et al., 2003; Lindsay and Rosenberg, 2011; Dhamala, 2008a,b). A recent article introduced a non-parametric framework for directionality analysis of bivariate data (Halliday, 2015), with application to single unit spike train data.

The concept of conditional independence is a powerful one that is widely used in partial regression models where the effects of variables that are believed to influence the correlation between dependent variables are removed to provide a more accurate description of any dependency (e.g. Ezekiel and Fox, 1958). The use of conditional causality measures to distinguish between direct and indirect influences has been considered in parametric approaches to directionality. Granger (1969) considers two and three variable models, leading in the three variable model case to a partial cross spectrum from which causal and feedback relationships between two variables conditioned on a third can be derived. An alternative parametric approach using information theoretic measures (Geweke, 1982) has also been extended to include conditioning variables (Pierce, 1982; Geweke, 1984). Related approaches are considered in Chen et al. (2006) and Guo et al. (2008).

This paper presents a novel extension to the non-parametric approach in Halliday (2015) for multivariate data by presenting a framework for analysis of three random processes. We also investigate applicability of the framework to both time series data and spike train data. One advantage of considering time series data is that measures derived from residual and conditional variance metrics can readily be calibrated against known (simulated) data. We undertake such a comparison to establish the accuracy and usefulness of our multivariate extension. The approach is further validated through application to experimental data consisting of local field potential recordings from bilateral hippocampus in anaesthetised rat. Our results demonstrate the flexibility of the non-parametric approach in dealing with both spike train and time series data. Our novel approach should therefore have broad applicability across a wide range of electrophysiological data.

The paper is arranged as follows. Section 2 presents the methods including sub-sections on algorithms and significance testing. Section 3 describes results from application of the conditional non-parametric framework to simulated cortical neuron networks, to artificial mixtures of Gaussian time-series used to verify quantitative aspects of the framework and to the experimental data. Conclusions and discussion are in Section 4.

2. Methods

Our framework assumes that random processes have wide-sense (weak) stationarity (Brillinger, 1975; Priestley, 1981). The approach can be applied to time series data and point-process data. Point process data are represented using differential increments which count the number of spikes in a small interval, which we assume to be the sampling interval Δt (Rosenberg et al., 1989; Conway et al., 1993). Point processes are also assumed to be orderly, i.e. only one spike can occur in each sampling interval (Conway et al., 1993). In the derivation below (x, y, z) refer to three random processes which can be either time series or point process differential increments, or mixtures of the two data types. We use the term multivariate in the manuscript, since we are considering the analysis of three simultaneous random processes. However, only a single predictor is used, the possibility of extending the analysis to multiple predictors is considered in the discussion.

2.1. Theory

For bivariate random processes (x, y) a scalar measure of overall dependence is given by the squared correlation coefficient (Pierce, 1979; Halliday, 2015). This is defined in terms of ordinary and residual variances as

$$R^2_{yx} = \frac{\sigma^2_y - \sigma^2_{y|x}}{\sigma^2_y} \tag{1}$$

The conditioned variance, $\sigma^2_{y|x}$ can be equated to the variance of the error process after a linear regression of y on x. Eq. (1) can be interpreted as the fraction of the variance in y that can be accounted for by the regressor x. It is a symmetrical measure which does not provide any indication of directionality of interaction.

To account for any common effect that process z may have on both x and y a partial correlation coefficient can be used

$$R^2_{yx|z} = \frac{\sigma^2_{y|z} - \sigma^2_{y|x,z}}{\sigma^2_{y|z}} \tag{2}$$

In this case both processes x and y are conditioned on the third process z. Partial regression is widely used in situations where it is believed that the predictor, z, can account for some or all of the original association between x and y. The objective is to distinguish a genuine correlation, $R^2_{yx|z}$, from an apparent or induced correlation, R^2_{yx}. Throughout this paper we use linear models and consider linear interactions.

The relationship between the scalar R^2_{yx} and the coherence function, $|R_{yx}(\lambda)|^2$ was used as the starting point for the derivation of non-parametric directionality measures in Halliday (2015). The frequency domain equivalent of the partial regression coefficient, Eq. (2), is the partial coherence function

$$|R_{yx|z}(\lambda)|^2 = \frac{|f_{yx|z}(\lambda)|^2}{f_{xx|z}(\lambda) f_{yy|z}(\lambda)} \tag{3}$$

where $f_{yx|z}(\lambda)$ is the partial cross power spectral density (or partial cross-spectrum) between processes x and y with predictor z. The two partial auto-spectra are $f_{xx|z}(\lambda)$ and $f_{yy|z}(\lambda)$. Partial coherence estimates have proved useful in identifying direct interactions from common inputs in functional connectivity studies of neural circuits (Rosenberg et al., 1998; Eichler et al., 2003; Salvador et al., 2005; Medkour et al., 2009).

The link between the partial coherence function in Eq. (3) and the partial correlation coefficient in Eq. (2) can be made by considering the residual variance in the partial regression model, $\sigma^2_{y|x,z}$. In the frequency domain this residual variance is the residual spectrum $f_{yy|x,z}(\lambda)$. Using the same derivation as the bivariate framework (Halliday, 2015) we can derive the result

$$\left|R_{yx|z}(\lambda)\right|^2 = \frac{f_{yy|z}(\lambda) - f_{yy|x,z}(\lambda)}{f_{yy|z}(\lambda)} \tag{4}$$

We have used the partial gain function (Halliday et al., 1995), $f_{yx|z}(\lambda)/f_{xx|z}(\lambda)$, in this derivation. Thus, as in the bivariate case, there is a close correspondence between the partial coherence function in Eq. (4) and the partial regression coefficient in Eq. (2). The partial coherence function decomposes the R^2 value by frequency, thus $R^2_{yx|z}$ can be recovered by integrating the partial coherence

$$R^2_{yx|z} = \frac{1}{2\pi} \int_{-\pi}^{+\pi} \left|R_{yx|z}(\lambda)\right|^2 d\lambda \tag{5}$$

where the partial coherence is defined over the normalised angluar frequency range $[-\pi, +\pi]$.

Application of the minimum mean square error (MMSE) pre-whitening step (Eldar and Oppenheim, 2003) is next applied to

reduce the partial coherence to the partial cross spectrum. Directionality measures can be derived using a similar sequence of steps as in the bivariate case (Halliday, 2015). The aim of the pre-whitening step is to reduce the two partial auto spectra to have the value 1 at each frequency in Eq. (3), which requires the application of two pre-whitening filters that must reflect the properties of the two processes x and y and their relationship to the predictor, z. This can be achieved using pre-whitened conditional discrete Fourier transforms as described below.

Auto spectra are traditionally defined in terms of the expectation operator as (Brillinger, 1975)

$$f_{xx}(\lambda) = \lim_{T\to\infty} \frac{1}{2\pi T} E\{d_x^T(\lambda)\bar{d_x^T}(\lambda)\} \tag{6}$$

$$f_{yy}(\lambda) = \lim_{T\to\infty} \frac{1}{2\pi T} E\{d_y^T(\lambda)\bar{d_y^T}(\lambda)\} \tag{7}$$

where $d_x^T(\lambda)$ and $d_y^T(\lambda)$ are the finite Fourier transforms of length T from processes x and y respectively, and the overbar indicates a complex conjugate. A finite Fourier transform conditioned on a third process, z, can be defined (Tick, 1963; Brillinger, 1988) as

$$d_{x|z}^T(\lambda) = d_x^T(\lambda) - \frac{f_{xz}(\lambda)}{f_{zz}(\lambda)} d_z^T(\lambda) \tag{8}$$

$$d_{y|z}^T(\lambda) = d_y^T(\lambda) - \frac{f_{yz}(\lambda)}{f_{zz}(\lambda)} d_z^T(\lambda) \tag{9}$$

The quantities $f_{xz}(\lambda)$, $f_{yz}(\lambda)$ and $f_{zz}(\lambda)$ are the two cross spectra between the conditioning process, z and the original processes and the auto spectra of z, respectively. Defining conditioned Fourier transforms in this manner allows the partial auto spectra to be defined as

$$f_{xx|z}(\lambda) = \lim_{T\to\infty} \frac{1}{2\pi T} E\{d_{x|z}^T(\lambda)\bar{d_{x|z}^T}(\lambda)\} \tag{10}$$

$$f_{yy|z}(\lambda) = \lim_{T\to\infty} \frac{1}{2\pi T} E\{d_{y|z}^T(\lambda)\bar{d_{y|z}^T}(\lambda)\} \tag{11}$$

The pre-whitening step is applied using an approach similar to the bivariate case presented in Halliday (2015). Extending the concept of the MMSE pre-whitening filter introduced in Eldar and Oppenheim (2003), we define the MMSE pre-whitening filters for the two partial spectra as

$$w_{xx|z}(\lambda) = f_{xx|z}(\lambda)^{-1/2} \tag{12}$$

$$w_{yy|z}(\lambda) = f_{yy|z}(\lambda)^{-1/2} \tag{13}$$

Using these filters the pre-whitened transforms can be generated as

$$dw_{x|z}^T(\lambda) = d_{x|z}^T(\lambda)\, w_{xx|z}(\lambda) \tag{14}$$

$$dw_{y|z}^T(\lambda) = d_{y|z}^T(\lambda)\, w_{yy|z}(\lambda) \tag{15}$$

Eqs. (14) and (15) mimic the frequency domain implementation applying pre-whitening filters to the processes x and y that was used in the bivariate case. The difference here is that the output of the filters are conditioned Fourier transforms which are optimally pre-whitened. Auto spectra estimated by replacing the expectation in Eqs. (10) and (11) with ensemble or segment averaging will have the value 1 at all frequencies:

$$f_{xx|z}^w(\lambda) = 1, \qquad f_{yy|z}^w(\lambda) = 1 \tag{16}$$

Estimation of the partial cross spectrum from the pre-whitened conditioned Fourier transforms, Eqs. (14) and (15), will be equivalent to the partial coherence

$$\left|R_{yx|z}^w(\lambda)\right|^2 = \left|f_{yx|z}^w(\lambda)\right|^2 \tag{17}$$

Conditioned directionality measures can then be derived from the pre-whitened partial cross spectrum, $f_{yx|z}^w(\lambda)$, in a manner similar to the bivariate case (Halliday, 2015). The overall scalar measure of dependence between x and y conditioned (linearly) on z, $R_{yx|z}^2$, is

$$R_{yx|z}^2 = \frac{1}{2\pi} \int_{-\pi}^{+\pi} |f_{yx|z}^w(\lambda)|^2 d\lambda \tag{18}$$

To decompose $R_{yx|z}^2$ by direction we define a correlation function, $\rho_{yx|z}(\tau)$ which is the inverse Fourier transform of the pre-whitened partial cross spectrum

$$\rho_{yx|z}(\tau) = \frac{1}{2\pi} \int_{-\pi}^{+\pi} f_{yx|z}^w(\lambda) e^{i\lambda\tau}\, d\lambda \tag{19}$$

The function defined in Eq. (19) could be referred to as a lagged conditional correlation function between x and y. Following Brillinger (1975), second order spectra are assumed periodic in λ with period 2π (Brillinger, 1975, Th 2.5.1). Decomposition of $R_{yx|z}^2$ by lag is achieved as

$$R_{yx|z}^2 = \int_{-\infty}^{+\infty} |\rho_{yx|z}(\tau)|^2 d\tau \tag{20}$$

The proof of this central result follows closely that for the bivariate case (Halliday, 2015), using Parseval's theorem (Priestley, 1981). Adopting the same approach as in the bivariate case allows the overall dependence to be decomposed summatively by direction

$$R_{yx|z}^2 = \int_{\tau<0} |\rho_{yx|z}(\tau)|^2 d\tau + |\rho_{yx|z}(0)|^2 + \int_{\tau>0} |\rho_{yx|z}(\tau)|^2 d\tau \tag{21}$$

which we write, with an obvious extension to the notation, as

$$R_{yx|z}^2 = R_{yx|z;-}^2 + R_{yx|z;0}^2 + R_{yx|z;+}^2 \tag{22}$$

In the frequency domain the decomposition also follows closely the approach adopted in the bivariate case. The f' measures are defined as

$$f'_{yx|z;-}(\lambda) = \int_{\tau<0} \rho_{yx|z}(\tau) e^{-i\lambda\tau}\, d\tau \tag{23}$$

$$f'_{yx|z;0}(\lambda) = \rho_{yx|z}(0) \tag{24}$$

$$f'_{yx|z;+}(\lambda) = \int_{\tau>0} \rho_{yx|z}(\tau) e^{-i\lambda\tau}\, d\tau \tag{25}$$

with decomposition of the partial coherence, $|R_{yx|z}(\lambda)|^2$, summatively at each frequency given by

$$|R_{yx|z}(\lambda)|^2 = |R'_{yx|z;-}(\lambda)|^2 + |R'_{yx|z;0}(\lambda)|^2 + |R'_{yx|z;+}(\lambda)|^2 \tag{26}$$

where the R' functions are scaled according to the relative magnitude of the f' functions at each frequency as

$$|R'_{yx|z;-}(\lambda)|^2 = \frac{|f'_{yx|z;-}(\lambda)|^2}{|f'_{yx|z;-}(\lambda)|^2 + |f'_{yx|z;0}(\lambda)|^2 + |f'_{yx|z;+}(\lambda)|^2} |R_{yx|z}(\lambda)|^2 \tag{27}$$

$$|R'_{yx|z;0}(\lambda)|^2 = \frac{|f'_{yx|z;0}(\lambda)|^2}{|f'_{y|zx;-}(\lambda)|^2 + |f'_{y|zx;0}(\lambda)|^2 + |f'_{yx|z;+}(\lambda)|^2} |R_{yx|z}(\lambda)|^2 \tag{28}$$

$$|R'_{yx|z;+}(\lambda)|^2 = \frac{|f'_{yx|z;+}(\lambda)|^2}{|f'_{yx|z;-}(\lambda)|^2 + |f'_{yx|z;0}(\lambda)|^2 + |f'_{yx|z;+}(\lambda)|^2} |R_{yx|z}(\lambda)|^2 \tag{29}$$

The validity of this decomposition in the bivariate case is discussed in Halliday (2015).

2.2. Algorithms

The directionality measures can be constructed as a straightforward extension to a typical multivariate spectral analysis. The conditional directionality measures, in this case, assume that three random processes, x, y and z, are available for analysis. The directionality measures are constructed using a two stage process. In the first stage the discrete Fourier transforms are calculated in the usual way, and estimates of second order spectra are calculated – these are the estimated auto spectra, $\hat{f}_{xx}(\lambda_j)$, $\hat{f}_{yy}(\lambda_j)$ and $\hat{f}_{zz}(\lambda_j)$, along with the estimated cross spectra, $\hat{f}_{yx}(\lambda_j)$, $\hat{f}_{xz}(\lambda_j)$ and $\hat{f}_{yz}(\lambda_j)$. Estimates are indicated through the use of the hat symbol, $\hat{}$, the λ_j are the Fourier frequencies, and the terminology for cross spectra, $\hat{f}_{yx}(\lambda_j)$, treats x as the reference (or input) process. A number of well documented approaches exist for construction of second order spectral estimates. Here we use the average periodogram approach, described in detail in Halliday et al. (1995), which involves sectioning a record into L sections each containing T data points, thus analysing a record of duration $R = LT$ samples. Alternatively, the directionality measures could be derived from alternative spectral estimation procedures, for example using multi-taper estimates (Percival and Walden, 1993).

The second stage constructs the conditional directionality estimates starting from the discrete Fourier transform for each segment, l ($l = 1, \ldots, L$), from processes x and y which are referred to as $d_x^T(\lambda_j, l)$ and $d_y^T(\lambda_j, l)$. The conditioned Fourier transforms for each segment are constructed as

$$d_{x|z}^T(\lambda_j, l) = d_x^T(\lambda_j, l) - \frac{\hat{f}_{xz}(\lambda_j)}{\hat{f}_{zz}(\lambda_j)} d_z^T(\lambda_j, l) \quad (l = 1, \ldots, L) \tag{30}$$

$$d_{y|z}^T(\lambda_j, l) = d_y^T(\lambda_j, l) - \frac{\hat{f}_{yz}(\lambda_j)}{\hat{f}_{zz}(\lambda_j)} d_z^T(\lambda_j, l) \quad (l = 1, \ldots, L) \tag{31}$$

This gives a conditioned Fourier transform for each segment, l, that is conditioned on the (common) process z. The conditioning factors (or gains) $\hat{f}_{xz}(\lambda_j)/\hat{f}_{zz}(\lambda_j)$ and $\hat{f}_{yz}(\lambda_j)/\hat{f}_{zz}(\lambda_j)$ are the same for each segment and use the spectral estimates constructed in the first stage analysis. The first order partial spectra are then estimated from the conditioned discrete Fourier transforms. Here an average is taken across segments, for process x this is

$$\hat{f}_{xx|z}(\lambda_j) = \frac{1}{2\pi LT} \sum_{l=1}^{L} |d_{x|z}^T(\lambda_j, l)|^2 \tag{32}$$

The $1/2\pi T$ factor follows the convention in the bivariate case. A similar expression is used to estimate $\hat{f}_{yy|z(\lambda_j)}$. The pre-whitening filters are constructed as

$$\hat{w}_{xx|z}(\lambda_j) = \hat{f}_{xx|z}(\lambda_j)^{-1/2} \tag{33}$$

$$\hat{w}_{yy|z}(\lambda_j) = \hat{f}_{yy|z}(\lambda_j)^{-1/2} \tag{34}$$

The hat indicates that these are estimates constructed from a single realisation of the three processes. A different realisation will result in a different pair of pre-whitening filters, this will achieve the objective of pre-whitening the conditioned auto-spectral estimates to 1 at each frequency. The pre-whitened discrete Fourier transforms for each segment, l are

$$dw_{x|z}^T(\lambda_j, l) = d_{x|z}^T(\lambda_j, l)\, \hat{w}_{xx|z}(\lambda_j) \quad (l = 1, \ldots, L) \tag{35}$$

$$dw_{y|z}^T(\lambda_j, l) = d_{y|z}^T(\lambda_j, l)\, \hat{w}_{yy|z}(\lambda_j) \quad (l = 1, \ldots, L) \tag{36}$$

Whitened partial auto and cross spectra are estimated using expressions similar to Eq. (32). To ensure that the whitened conditional auto spectral estimates, $\hat{f}_{xx|z}^w(\lambda)$ and $\hat{f}_{yy|z}^w(\lambda)$, have the value 1 at all frequencies, the same averaging (or weighted averaging) should be applied to the same data segments when calculating the whitened spectra. The partial coherence can then be obtained directly from the whitened partial cross spectrum as

$$|\hat{R}_{yx|z}^w(\lambda_j)|^2 = |\hat{f}_{yx|z}^w(\lambda_j)|^2 \tag{37}$$

From this the partial correlation function, $\rho_{yx|z}(\tau)$, is estimated using a standard inverse Fourier transform of length T (Halliday et al., 1995).

The estimation of the directional metrics, the overall measure $R_{yx|z}^2$ and directional components $R_{yx|z;-}^2$, $R_{yx|z;0}^2$ and $R_{yx|z;+}^2$ are estimated from $\hat{\rho}_{yx|z}(\tau_k)$ using the same algorithms as in the bivariate case, by substituting $\hat{\rho}_{yx|z}(\tau_k)$ for $\hat{\rho}_{yx}(\tau_k)$ (Halliday, 2015). The same substitution allows the estimated f' functions, $\hat{f}'_{yx|z;-}(\lambda_j)$, $\hat{f}'_{yx|z;0}(\lambda_j)$ and $\hat{f}'_{yx|z;+}(\lambda_j)$, to be obtained from $\hat{\rho}_{yx|z}(\tau_k)$ and from these the estimated conditioned directional coherence functions, $|\hat{R}'_{yx|z;-}(\lambda_j)|^2$, $|\hat{R}'_{yx|z;0}(\lambda_j)|^2$ and $|\hat{R}'_{yx|z;+}(\lambda_j)|^2$ by direct substitution of the appropriate estimates into Eqs. (27)–(29). Algorithmic level descriptions of the conditional, three variable, analysis and the unconditional, two variable (Halliday, 2015) analysis are given in Appendix.

2.3. Significance testing

The approach here follows that adopted in the bivariate case (Halliday, 2015). The scalar measure of overall conditional correlation, $R_{yx|z}^2$ is estimated by integration of partial coherence estimates. Confidence limits on partial coherence estimates are used as an indicator of a statistically significant interaction. The setting of significance levels for partial coherence estimates constructed using average periodograms over L segments can be found in Brillinger (1975), Rosenberg et al. (1989) and Halliday et al. (1995). In particular an upper 95% confidence limit based on a null hypothesis of no correlation after removal of common linear effects from a single predictor can be estimated as (Rosenberg et al., 1989)

$$1 - 0.05^{1/(L-2)} \tag{38}$$

This confidence limit can be used to assess the significance of $\hat{R}_{yx|z}^2$. We assume that significant values of $\hat{R}_{yx|z}^2$ will result when the corresponding partial coherence estimate has significant values (at frequencies of interest).

The variance of the bivariate correlation function, $\rho_{yx}(\tau)$, was considered in Halliday (2015). The expression involved integration over the product of the prewhitened spectra, which have the value 1 at all frequencies. We use the same approach for the multivariate correlation function, except that the integration is over the product of the two pre-whitened partial spectra $f_{xx|z}^w(\lambda)$ and $f_{yy|z}^w(\lambda)$. Since these are similarly equal to 1 at all frequencies we obtain the same result $var\{\rho_{yx|z}(\tau)\} = 1/R$. Approximate upper and lower 95% confidence limits can be set as

$$0 \pm \frac{1.96}{\sqrt{R}} \tag{39}$$

where $R = LT$, the total number of points analysed. The interpretation in the multivariate case is similar to that for the bivariate case. Significant values of $\hat{\rho}_{yx|z}(\tau)$ at lags $\tau < 0$ indicates a significant $R_{yx|z;-}^2$, and significant values of $\hat{\rho}_{yx|z}(\tau)$ at lags $\tau > 0$ indicates a significant $R_{yx|z;+}^2$. A significant value of $\hat{\rho}_{yx|z}(0)$ indicates a significant $R_{yx|z;0}^2$.

The validity of Eq. (39) was checked using Monte-Carlo simulations using three examples of time series data (rows 1, 3, 5 from Table 1) and three examples of spike train data (configurations

Table 1
Theoretical values of R^2_{yx} and mean and range (mean ± 2SD) of $\hat{R}^2_{yx}$ and $\hat{R}^2_{yx|z}$ for simulated time series where the correlation between x and y is due entirely to the common influence of process z used as predictor in the conditional directionality analysis. The target value of $R^2_{yx|z}$ is zero in all cases. Metrics calculated from 100 trials, each trial used 100 segments with 2^{10} samples per segment.

R^2_{yx}	$\hat{R}^2_{yx}$	$\hat{R}^2_{yx}$ range	$\hat{R}^2_{yx|z}$	$\hat{R}^2_{yx|z}$ range
0.1	0.108	0.105, 0.111	0.01	0.0091, 0.0110
0.3	0.305	0.301, 0.309	0.01	0.0092, 0.0110
0.5	0.502	0.500, 0.505	0.01	0.0092, 0.0110
0.7	0.700	0.698, 0.702	0.01	0.0092, 0.0107
0.9	0.899	0.899, 0.900	0.01	0.0092, 0.0110

a and b from Fig. 1 and 1 set of Poisson spike trains). In each example 100 repeat runs were undertaken with parameters $L = 97$ and $T = 1024$ and the percentage of points in estimates of $\hat{\rho}_{yx|z}(\tau)$ above and below the confidence limits calculated using Eq. (39) calculated. The percentage of values outside the upper and lower 95% confidence limits ranged from 5.03% to 5.19%, suggesting good agreement with Eq. (39). In addition Q–Q plots of the simulated data against an assumed $\mathcal{N}(0, 1)$ distribution (not shown) further suggest the assumptions behind Eq. (39) are reasonable. Interestingly these Monte-Carlo simulations highlighted a small bias in the point-process case where the distribution of values outside the [lower, upper] confidence limits is around [2, 3]% instead of the expected [2.5, 2.5]%. The reason for this bias may be related to applying the same assumptions to time series and point process data as it only affects analysis of spike trains. It is of the order of 0.5%, large scale studies should take this additional bias into account, however, it should have limited impact on interpretation of individual records.

3. Results

The conditional directionality measures are applied to simulated and experimental data. The first set of simulations uses the same three cortical neuron networks that were used to validate the bivariate measures. Application to simulated time series data uses three correlated random processes (mixtures of Gaussian noise with and without additional delays), these simple times series models have the advantage of known, theoretical correlation values and are used as a validation of the $R^2_{yx|z}$ conditional directionality measures and estimates of the conditional directional coherence, $|R'_{yx|z;.}(\lambda)|^2$ functions. Application to experimental data is illustrated through analysis of a data set consisting of simultaneous bilateral recordings of local field potentials from CA1 and CA3 in the rat.

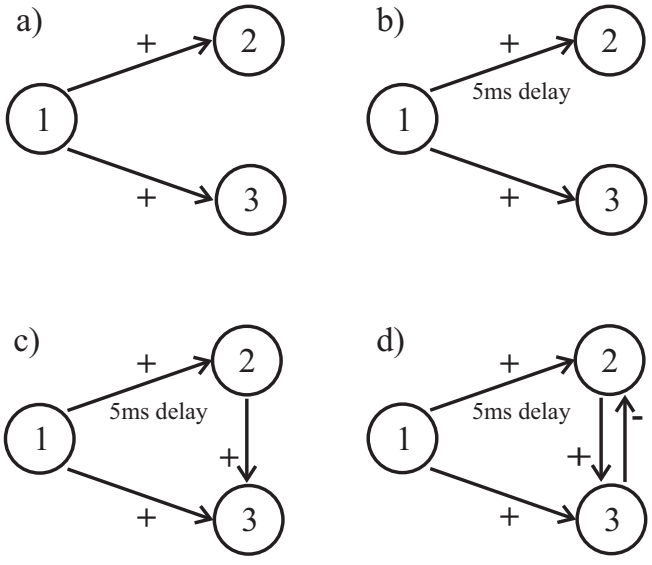

Fig. 1. Network configuration for cortical network simulations. Excitatory connections are indicated: "+", inhibitory connections are indicated: "–". In configurations (b)–(d) the connection from 1 → 2 has an additional synaptic delay of 5 ms.

3.1. Simulated 3 neuron networks

The configurations that are used are illustrated schematically in Fig. 1. The neurons are simulated cortical neurons (Troyer and Miller, 1997), the neuron parameters, large scale background synaptic activation parameters and dynamics of the connections from 1 → 2 and 1 → 3 are the same as and described in detail in Halliday (2015). In brief, the model neurons have a time constant of 20 ms, and all receive independent excitatory and inhibitory inputs, 4000 excitatory inputs/s, 300 μV EPSPs and 1000 inhibitory inputs/s, shunting inhibition, simulating the balanced large scale background synaptic activation seen *in vivo* (Destexhe et al., 2003). The common excitatory inputs from 1 → 2 and 1 → 3 have 2000 μV EPSPs and in configurations (b), (c) and (d) an additional synaptic conduction delay of 5 ms is included from 1 → 2 in addition to the existing synaptic conduction process. Synaptic delays are an important component of neural circuits, they are included here to test the ability of the non-parametric directionality framework to correctly infer direction in the presence of delays. Configurations (a) and (b) have no direct connections between neurons 2 and 3, thus the correlation which is induced by the common inputs from neuron 1 should be removed in the conditional directionality analysis when using the spikes from neuron 1 as the predictor. Configurations (c) and (d) have direct connections between neurons 2 and 3, the results below investigate whether the conditional directionality estimates accurately capture the features of these direct connections after removing the common influence of the spikes from neuron 1.

Fig. 2 illustrates the bivariate time domain analysis between the firing sequences of neurons 2 and 3. These figures were generated

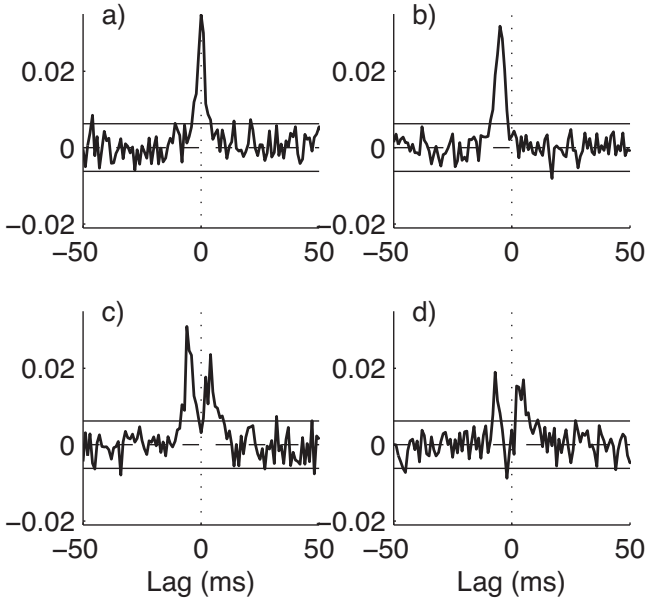

Fig. 2. Bivariate directionality analysis for interactions between neurons 2 and 3. Configurations as shown in Fig. 1. Plots show the estimated correlation function, $\hat{\rho}_{32}(\tau)$, along with null value (dashed horizontal line at zero) and upper and lower 95% confidence limits (solid horizontal lines) based on the assumption of uncorrelated processes. The lag ranges are the same for all panels, a dotted vertical line at $\tau = 0$ is included for reference.

from a single sample record of duration 100 s. The firing rate of all neurons varied from 10.5 to 18 spikes/s, and the coefficient of variation varied from 0.69 to 0.78, over the four examples illustrated. The four estimates in Fig. 2 show the estimated bivariate correlation, $\hat{\rho}_{32}(\tau)$, between neurons 2 and 3, with neuron 2 the reference. Configuration (a) has no connection between neurons 2 and 3, however, the common input does induce an apparent correlation between the two neurons. This is seen as a significant peak centred around time zero. Configurations (b)–(d) have the same pattern of common inputs as configuration (a), except with an additional delay of 5 ms from $1 \rightarrow 2$ which induces an apparent directionality from $2 \leftarrow 3$. This is observed as the peak in the unconditional estimate $\hat{\rho}_{32}(\tau)$ at negative values of lag τ in Fig. 2b–d. Configurations (c) and (d) also have excitatory connections from $2 \rightarrow 3$ this appears as an additional peak in $\hat{\rho}_{32}(\tau)$ at positive values of τ in Fig. 2c and d. Configuration (d) has an additional inhibitory connection from $2 \leftarrow 3$, we would expect to see a depression at negative lags in Fig. 2d, however there is little evidence of this as it is masked by the apparent excitatory association induced by the common input from neuron 1. Thus the unconditional directionality analysis does not provide an accurate indication of the interactions between neurons 2 and 3.

Fig. 3 shows the estimated conditional correlation function, $\hat{\rho}_{32|1}(\tau)$, here the interaction between neurons 2 and 3 is conditioned on the spike timings from neuron 1. The configuration, lag range and the individual vertical axes in each plot are the same as in Fig. 2. Configurations (a) and (b) have no direct connection between neurons 2 and 3, thus we would expect to see a conditional directionality estimate that is not significantly different from zero. This is the case in Fig. 3a and b where there is no evidence of any relationship. Configuration (c) has a single excitatory connection from $2 \rightarrow 3$. The conditional estimate in Fig. 3c has a significant peak at positive lags in $\hat{\rho}_{32|1}(\tau)$, in agreement with Fig. 1c. Configuration (d) has an excitatory connection from $2 \rightarrow 3$ and an inhibitory connection from $2 \leftarrow 3$. Both these are connections are accurately captured by the estimate in Fig. 3d, in particular removal of the common input to neurons 2 and 3 has unmasked the inhibitory connection (compare Fig. 3d with Fig 2d), there is now a clear, significant depression at negative time lags in $\hat{\rho}_{32|1}(\tau)$ in Fig. 3d.

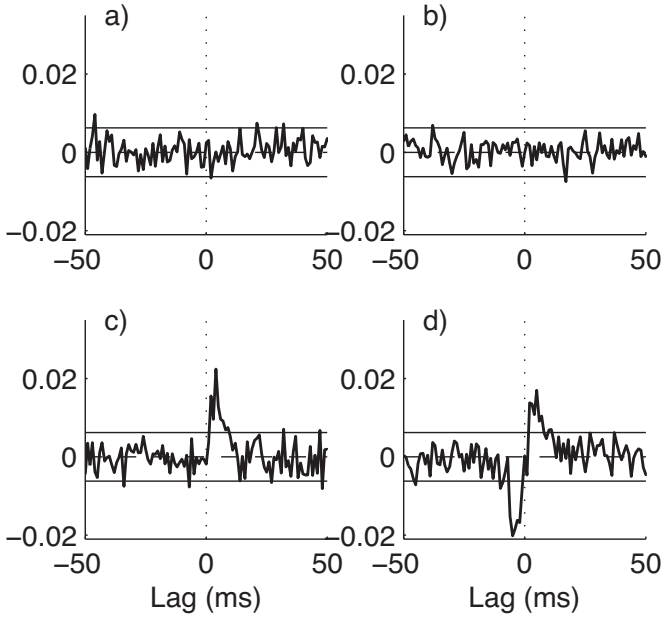

Fig. 3. Conditional directionality analysis for interactions between neurons 2 and 3, conditioned on neuron 1. Configurations as shown in Fig. 1. Plots show the estimated conditional correlation function, $\hat{\rho}_{32|1}(\tau)$, along with null value (dashed horizontal line at zero) and upper and lower 95% confidence limits (solid horizontal lines) based on the assumption of uncorrelated processes. The lag ranges are the same for all panels, the vertical axes are the same as the corresponding plot in Fig. 2. A dotted vertical line at $\tau = 0$ is included for reference.

Table 2
Theoretical values of R^2_{yx} (column 1) and $R^2_{yx|z}$ (column 4) and mean and range (mean ± 2SD) of $\hat{R}^2_{yx}$ and $\hat{R}^2_{yx|z}$ for simulated time series where the correlation between x and y is partly accounted for by the common influence of process z used as predictor in the conditional directionality analysis. Metrics calculated from 100 trials, each trial used 100 segments with 2^{10} samples per segment.

R^2_{yx}	$\hat{R}^2_{yx}$	$\hat{R}^2_{yx}$ range	$R^2_{yx\|z}$	$\hat{R}^2_{yx\|z}$	$\hat{R}^2_{yx\|z}$ range
0.4	0.403	0.399, 0.407	0.30	0.303	0.299, 0.308
0.4	0.403	0.399, 0.407	0.21	0.220	0.216, 0.224
0.5	0.502	0.498, 0.506	0.39	0.398	0.394, 0.402
0.5	0.502	0.498, 0.506	0.11	0.114	0.112, 0.117
0.6	0.601	0.598, 0.604	0.40	0.403	0.400, 0.406
0.6	0.601	0.598, 0.604	0.17	0.173	0.169, 0.176
0.8	0.800	0.798, 0.802	0.65	0.655	0.653, 0.658
0.8	0.800	0.798, 0.801	0.40	0.399	0.396, 0.402

3.2. Application to time series with known correlation structure

This section considers application of the conditional directionality metrics and functions to simulated time series data. The data are generated using combinations of white noise, from iid $\mathcal{N}(0, 1)$, with known weights and delays. The first set consists of three random processes, where the bivariate correlation between x and y is entirely due to the common effects of process z, used as predictor in the conditional directionality analysis. The results are summarised in Table 1 which gives the theoretical (target) values for R^2_{yx}, the mean and range (mean ± 2SD) of the estimates $\hat{R}^2_{yx}$ and $\hat{R}^2_{yx|z}$. Values were estimated from 100 independent trials, where each trial used 100 segments of length 2^{10} samples.

The second set consists of a similar analysis, except in this case the theoretical (or target) conditional correlation, $R^2_{yx|z}$, differs from zero. Here x and y were generated from a mixture of Gaussian model as in Table 1, except two processes were common to both x and y, only one is the predictor z, thus the residual correlation $R^2_{yx|z}$ is non-zero. The results are summarised in Table 2 which also includes the target and estimated residual correlation, all configurations have non-zero target values of R^2_{yx} and $R^2_{yx|z}$. The results in Tables 1 and 2 suggest that estimates of the conditional directionality metric, $R^2_{yx|z}$ can usefully distinguish direct interactions from common effects in multivariate time series.

The results presented in Table 2 use an instantaneous mixing of signals to generate the dependencies, thus coherence, directional coherence and conditional directional coherence estimates are constant at all frequencies. Introduction of delays into the generation of the processes x and y will modulate the bivariate relationship across frequency, which should be removed in the conditional estimates. The next example considers this scenario using two random processes generated according to the model: $x(t) = a_1 z_1(t-1) + a_2 z_2(t) + \sqrt{1-(a_1^2+a_2^2)}\varepsilon_1(t)$ and $y(t) = a_1 z_1(t) + a_2 z_2(t-1) + \sqrt{1-(a_1^2+a_2^2)}\varepsilon_2(t)$, where the four random processes z_1, z_2, ε_1 and ε_2 are iid $\mathcal{N}(0, 1)$, and $(a_1^2 + a_2^2) < 1$. The coherence is $|R_{yx}(\lambda)|^2 = a_1^4 + a_2^4 + 2a_1^2 a_2^2 \cos(2\lambda)$, here λ is radian frequency. The directional components are $|R'_{yx;-}(\lambda)|^2 = a_1^4(a_1^4 + a_2^4)^{-1}|R_{yx}(\lambda)|^2$ and $|R'_{yx;+}(\lambda)|^2 = a_2^4(a_1^4 + a_2^4)^{-1}|R_{yx}(\lambda)|^2$, these can be derived from Halliday (2015, Eqs. (2.18), (2.20)). The two partial coherence estimates are $|R_{yx|z_1}(\lambda)|^2 = a_2^4(1-a_1^2)^{-2}$ and $|R_{yx|z_2}(\lambda)|^2 = a_1^4(1-a_2^2)^{-2}$, respectively. This example should demonstrate an unmasking effect in the partial coherence estimates, which are constant over frequency, compared with the

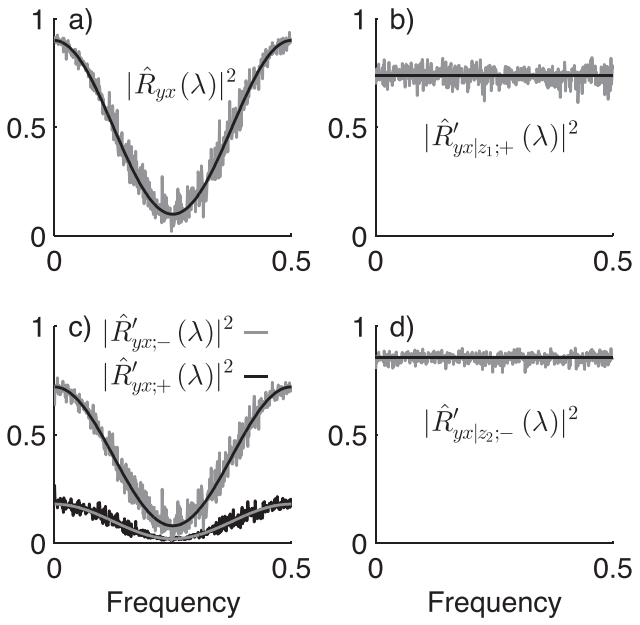

Fig. 4. Conditional and unconditional directionality analyses of the relationship between four simulated processes, z_1, z_2 (predictors) and x, y. (a) Estimated ordinary coherence between x and y (grey) compared with theoretical model (black). (b) Estimated forward component of conditional coherence estimate with z_1 as predictor (grey) compared with theoretical model (black). (c) Estimated forward (black) and reverse (grey) components of coherence estimate in panel (a). The theoretical values are shown in grey and black for forward and reverse estimates, respectively. (d) Estimated reverse component of conditional coherence estimate with z_2 as predictor (grey) compared with theoretical model (black). Plots are shown against fractional frequency where 0.5 corresponds to the Nyquist frequency. See text for parameters and further details.

ordinary coherence which is modulated over frequency. Fig. 4 illustrates analysis of a single trial, using 100 segments of length 2^{10} points generated using this model for x and y with parameters $a_1 = \sqrt{2/3\sqrt{0.9}}$ and $a_2 = \sqrt{1/3\sqrt{0.9}}$.

For these parameters the coherence at zero frequency is $|R_{yx}(0)|^2 = 0.9$. The two partial coherence functions are $|R_{yx|z_1}(\lambda)|^2 = 0.74$ and $|R_{yx|z_2}(\lambda)|^2 = 0.855$, independent of frequency. The differential delays used in the generation of $x(t)$ and $y(t)$ will induce directionality into the pattern of dependencies. Common input z_1 influences y before x thus induces directionality $x \leftarrow y$, in contrast common input z_2 induces directional interaction $x \rightarrow y$. Thus the ordinary coherence should have components in the forward and reverse direction and we would expect to see non-zero $|\hat{R}'_{yx;+}(\lambda)|^2$ and $|\hat{R}'_{yx;-}(\lambda)|^2$. In the conditional case the residual correlation after removal of z_1 will be in the forward direction, $x \rightarrow y$, thus $|\hat{R}'_{yx|z_1;+}(\lambda)|^2$ should agree with $|R_{yx|z_1}(\lambda)|^2$. The residual correlation after removal of z_2 will be in the reverse direction, $x \leftarrow y$, thus $|\hat{R}'_{yx|z_2;-}(\lambda)|^2$ should agree with $|R_{yx|z_1}(\lambda)|^2$.

The results in Fig. 4 are in good agreement with these expectations. Fig. 4a shows the ordinary coherence estimate (grey) against the theoretical curve (black). There is good agreement. The other three panels explore how the non-parametric directionality measures capture the unconditional and conditional relationship between x and y. Fig. 4c shows the two bivariate directionality estimates, forward $|\hat{R}'_{yx;+}(\lambda)|^2$ (black), and reverse $|\hat{R}'_{yx;-}(\lambda)|^2$ (grey). These two estimates sum to give the coherence estimate in Fig. 4a. Both estimates agree with the theoretical directional components shown superimposed on each trace. The induced interaction is stronger in the reverse direction, since $a_1 > a_2$ in the above time series model. Fig. 4b shows the constant theoretical $|R_{yx|z_1}(\lambda)|^2$, 0.74 (black) and the estimated conditional forward coherence estimate $|\hat{R}'_{yx|z_1;+}(\lambda)|^2$ (grey). There is good agreement between these two, the other estimated directional components, $|\hat{R}'_{yx|z_1;-}(\lambda)|^2$ and $|\hat{R}'_{yx|z_1;0}(\lambda)|^2$ are negligible (not shown). Similarly in Fig. 4d there is good agreement between the theoretical $|R_{yx|z_2}(\lambda)|^2 = 0.855$ (black) and the estimated $|\hat{R}'_{yx|z_2;-}(\lambda)|^2$ (grey), where the conditional directional analysis correctly identifies the interaction in the reverse direction. The other estimated directional components $|\hat{R}'_{yx|z_2;+}(\lambda)|^2$ and $|\hat{R}'_{yx|z_2;0}(\lambda)|^2$ are negligible (not shown). Thus, the unconditional and conditional directionality analysis is able to correctly infer the strength and direction between the four simulated processes z_1, z_2, x and y.

3.3. *Application to bilateral hippocampal* in vivo *recordings – bivariate directionality analysis*

This section describes application of the bivariate directionality analysis to local field potential (LFP) recordings from bilateral Hippocampus (HPC). The data is from a larger study investigating intra- and inter-hippocampal connectivity in a model of kainic acid (KA) induced mesial temporal lobe epilepsy (mTLE) in rat (Senik et al., 2013). Isoflurane anaesthetised Lister-hooded rats (300–400 g) had microelectrode arrays positioned in the left and right hippocampus. A cannula was attached to the left electrode for local injection of saline or kainic acid (1 mM, 1 μL) following a 30 min basal period. Multiple single-unit and local field potential activity (LFPs; filtered at 0.07–300 Hz) were recorded simultaneously using a Plexon Multichannel Acquisition Processor (MAP) system, see Coomber et al. (2008) for further details. All procedures had ethical approval and were carried out in accordance with the Animals (Scientific Procedures) Act 1986, UK.

The approach is applied to a single record of duration 211 min. Here we consider bivariate directionality analysis between simultaneous LFP records in CA1 and CA3 hippocampal regions in each hemisphere. Fig. 5 shows the estimated coherence ($|\hat{R}_{yx}(\lambda)|^2$, top) and the forward ($|\hat{R}'_{yx;+}(\lambda)|^2$, middle) and reverse ($|\hat{R}'_{yx;-}(\lambda)|^2$, lower) components for CA3–CA1 in left hemisphere. Fig. 6 shows the estimates for CA3–CA1 in the right hemisphere, in both cases CA3 region is the reference. The complete record was split into blocks for analysis, these blocks consisted of 58 segments of length 1024 points. Each block was analysed separately and bivariate directionality parameters calculated as described in Halliday (2015). Adjacent blocks were non-overlapping. Each block is approximately 1 min in duration, 59.39 s, with sampling rate 1 ms.

Both sets demonstrate strong coherence between CA3 and CA1 LFP signals, and exhibit a modulation of the coherence and the directional components after application of KA. Both the strength of coherence and range of frequencies change after KA is applied. This can be seen more clearly in the sections illustrated in Figs. 7 and 8. These illustrate the frequency (left) and time domain (right) bivariate directionality analysis for fixed blocks 6 (top; pre-KA injection), 50 (middle; soon after KA injection) and 150 (lower; well after KA injection), respectively, corresponding to ∼1 min blocks centred at 5.4, 49 and 148 min into the data set. These figures represent vertical sections through the time-frequency plots in Figs. 5 and 6, at fixed times.

For the left (ipsilateral) side the overall strength of interaction between CA3 and CA1 decreases after local injection of KA. The range of frequencies that exhibit significant coherence decreases from 200 Hz (block 6) to 125 Hz and 115 Hz (blocks 50 and 150, respectively). The interaction tends to become more balanced, the percentage of $\hat{R}^2_{yx;200}$, the overall strength of correlation at frequencies up to 200 Hz, in the forward direction remains constant at 54%, the percentage in the reverse direction increases from 22% in block 6 to 32% in block 50 and 36% in block 150, accompanied

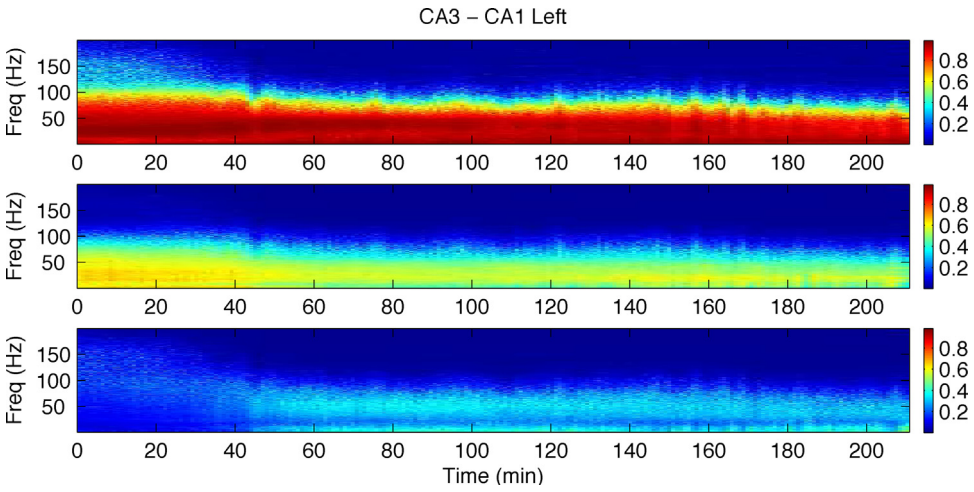

Fig. 5. Bivariate directionality analysis of LFP recordings from CA3 and CA1 in left hippocampus in an anaesthetised rat. Kainic acid was injected locally into the left hippocampus at 30 min. The plots show the estimated coherence (top) and forward (CA3 → CA1, middle) and reverse (CA3 ← CA1, bottom) components, with CA3 as the reference. Analysis was undertaken by splitting the complete record in to non-overlapping blocks of duration approximately 1 min. Scale bars on the right indicate the strength of coherence (top) and directional (middle, bottom) components, all to the same scale. The 95% significance level for the coherence estimate (top) is 0.0512, based on the assumption of uncorrelated signals.

by a decrease in the percentage at zero lag. For this data, the frequencies where the directional components are strongest are not those where the original coherence is strongest. For the left side, the forward component (red) peaks at lower frequencies, whereas the reverse component (blue) peaks at higher frequencies than the ordinary coherence. In block 6 the ordinary coherence peaks around 30 Hz, the forward component peaks around 20 Hz and the reverse component peaks at frequencies >100 Hz. In block 150 the coherence and forward component have peaks at similar frequencies to block 6, whereas the reverse component has a peak around 50 Hz.

Injection of local KA into the left hemisphere also modulates the interaction between the CA3 and CA1 LFP signals in the right hemisphere as shown by the sections in Fig. 8. The range of frequencies that exhibit significant coherence decreases from 110 Hz (block 6) to 85 Hz and 75 Hz (blocks 50 and 150, respectively). The interaction tends to become more one directional, the percentage of $\hat{R}^2_{yx;200}$, in the forward direction increases from 67% in block 6 to 86% in block 50 and 90% in block 150. For the right side in block 6 the coherence and forward components both have peaks around 30 Hz, in contrast the reverse component has a peak around 50 Hz. In later sections the magnitude of the reverse component is greatly reduced thus the forward component is very similar to the ordinary coherence, in block 150 the maximum is around 20 Hz.

The time domain estimates (right column) gives further insight into the characteristics of the interaction between CA3 and CA1. The positive peak in $\hat{\rho}_{yx}(\tau)$ indicates a latency of around 3–4 ms from CA3 → CA1. In the basal section (block 6) an interaction can be seen in the opposite direction, CA3 ← CA1, this has a similar latency of around 3 ms. Interestingly this feature has negative magnitude (Fig. 8b, negative lag) suggestive of an inhibitory effect. The application of KA abolished this CA3 ← CA1 interaction in the contralateral HPC (Fig. 8d, f). The results demonstrate that unilateral local KA injection has a marked effect on the strength and directionality of interaction between CA3 and CA1 in both left and right HPC. The KA appears to have different effects on each hemisphere, the strength of CA3 ← CA1 interaction increases in the ipsilateral (left) hemisphere (Fig. 7, blue lines), whereas it reduces in the contralateral (right) hemisphere (Fig. 8, blue lines).

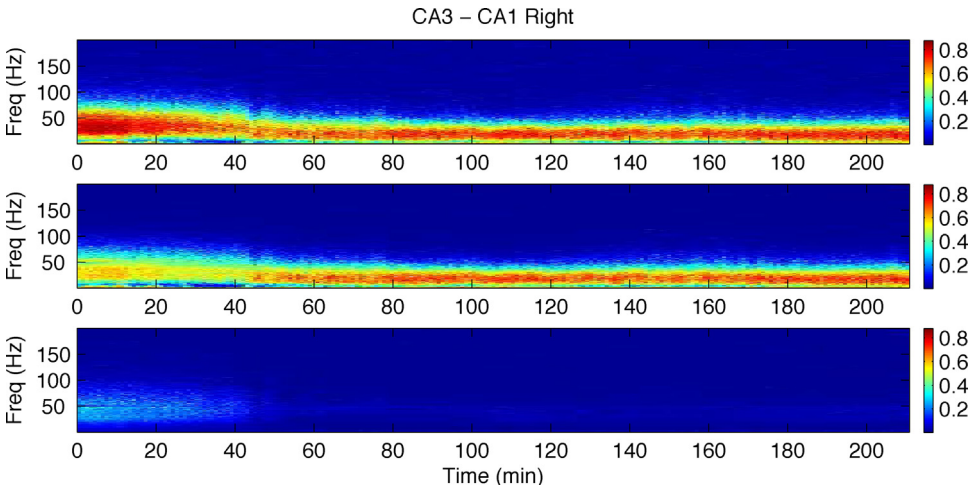

Fig. 6. Bivariate directionality analysis of LFP recordings from CA3 and CA1 in right hippocampus in an anaesthetised rat. Kainic acid was injected into the left hippocampus after 30 min basal recording. The plots show the estimated coherence (top) and forward (middle) and reverse (bottom) components, with CA3 as the reference. Analysis used same parameters as for left hippocampus, see legend for Fig. 5.

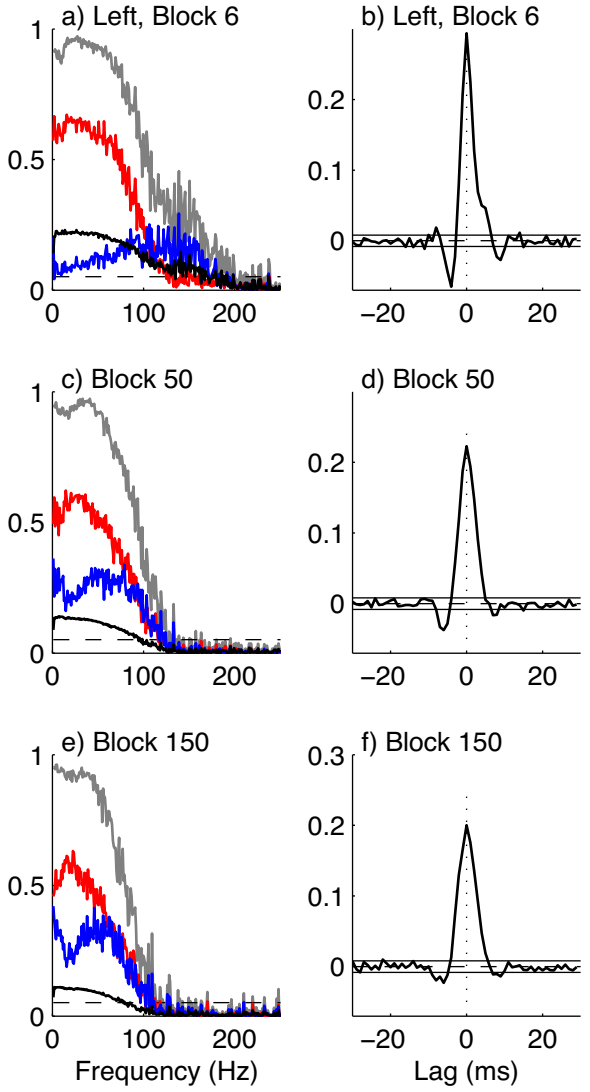

Fig. 7. Directionality analysis for ∼1 min blocks centred at 5.4 (block 6, top), 49 (block 50, centre) and 148 min (block 150, lower). Analysis is for CA3–CA1 interaction in left hemisphere (CA3–CA1, L), ipsilateral to local KA injection. Left column shows frequency domain analysis, with coherence (grey), forward component (red), reverse component (blue) and zero lag component (black). The dashed horizontal line is the estimated upper 95% confidence limit for the coherence based on the assumption of uncorrelated signals. Right column illustrates time domain analysis showing estimated correlation function, along with null value (dashed horizontal line) and upper and lower 95% confidence limits based on the assumption of uncorrelated signals. Further discussion in text. (For interpretation of the references to colour in this figure legend, the reader is referred to the web version of this article.)

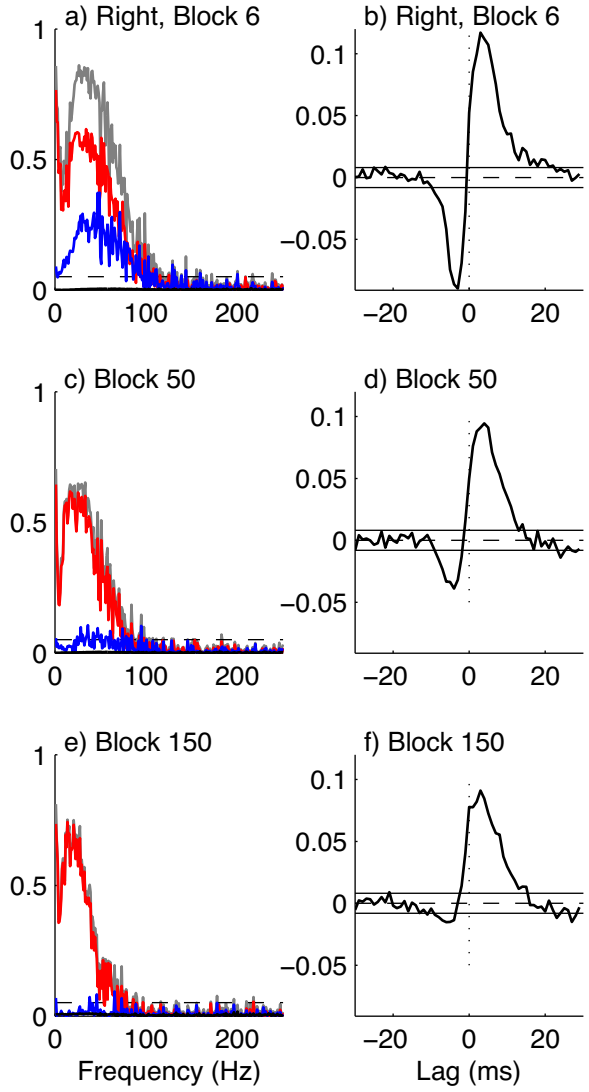

Fig. 8. Directionality analysis for ∼1 min blocks centred at 5.4 (block 6, top), 49 (block 50, centre) and 148 min (block 150, lower). Analysis is for hippocampal CA3–CA1 interaction in the right hemisphere (CA3–CA1, R), contralateral to local KA injection. Layout, format and confidence limits same as in Fig. 7. Further discussion in text. (For interpretation of the references to colour in this figure legend, the reader is referred to the web version of this article.)

These effects persist for the duration of the available record, 3 h post-injection.

4. Discussion

This article presents two important developments to the non-parametric directionality framework in Halliday (2015). The first is the development of conditional directionality measures, the second considers applicability to time series data. Conditional measures are derived by decomposing the MMSE pre-whitened (Eldar and Oppenheim, 2003) partial coherence in the same manner as the unconditional measures decompose the ordinary coherence (Halliday, 2015). The MMSE pre-whitening step ensures equality between the partial cross spectrum and partial coherence, Eq. (17), allowing the conditional scalar measure of dependence, $R^2_{yx|z}$, to be determined by integration of the pre-whitened partial cross spectrum $f^w_{yx|z}(\lambda)$, Eq. (18). Estimates of this, and the decomposition into three directional components, $R^2_{yx|z;-}$, $R^2_{yx|z;0}$ and $R^2_{yx|z;+}$, provide scalar measures of linear association, on a scale from 0 to 1, of the interaction between processes (x, y) after taking into account any common linear influence from process z. An additional set of functions, $|R'_{yx|z;-}(\lambda)|^2$, $|R'_{yx|z;0}(\lambda)|^2$ and $|R'_{yx|z;+}(\lambda)|^2$ decompose the partial coherence summatively into reverse, zero lag, and forward components, Eq. (26), in an analogous manner to that for the ordinary coherence in Halliday (2015). A complementary time domain partial correlation function, $\rho_{yx|z}(\tau)$ provides a time domain view of the conditional dependence between x and y with predictor z.

The concept of partial coherence is not new (Tick, 1963), it has been used as a technique to infer neuronal connectivity that can distinguish common inputs from direct connections (Rosenberg et al., 1989, 1998; Eichler et al., 2003; Halliday, 2005; Salvador et al., 2005; Medkour et al., 2009). The novelty here is to incorporate non-parametric directionality measures into partial coherence functions of order one. This conditioning on a predictor

allows the partial coherence, and its decomposition by direction, to correctly infer the connectivity in the simulated cortical neuron networks in Fig. 1, compare Fig. 3 with Fig. 2, by removing the common influence from neuron 1 onto neurons 2 and 3. Applicability of the framework to time series follows in a direct way from the discussions on analysis of hybrid data (mixed time series and point process) in Brillinger (1974), Halliday et al. (1995). The relationship between our non-parametric approach and parametric and other non-parametric approaches is discussed in Halliday (2015), these comments also apply to the conditional case considered here. The results using simulated data in Tables 1 and 2 demonstrate that the unconditional and conditional non-parametric directionality measures correctly infer the relationship between simulated time series signals generated from mixtures of Gaussians. Partial coherence analysis of spike train data using up to 7 predictors, and of human EEG using up to 8 predictors is presented in Halliday (2005) and Medkour et al. (2009), respectively. Partial coherence analysis of neural spike trains can distinguish between direct and indirect connections, increasing numbers of predictors can give a more accurate representation of synaptic interactions (Eichler et al., 2003). Future work will consider how the MMSE pre-whitening step can be extended to allow partial coherence estimates of order greater than 1 to be decomposed by direction.

The framework is applied to experimental times series data using LFP records from bilateral hippocampus in anaesthetised rat. Figs. 5 and 6 show how the directionality changes over the 211 min record in response to local injection of kainic acid to induce epileptiform activity after 30 min. Figs. 7 and 8 illustrate a bivariate directionality analysis at fixed points before and after application of kainic acid and demonstrate systematic changes in the pattern and direction of interaction between CA1 and CA3 LFP signals in each hemisphere in response to drug injection. Changes in overall correlation and directionality can be quantified if necessary using the scalar metrics defined in Eq. (22). A more detailed analysis of this data will be presented elsewhere including non-parametric conditional analysis of the intra and inter hemispheric interactions.

In this paper we have introduced a non-parametric approach to estimate conditional directionality. The analysis decomposes the partial coherence by direction of interaction, providing a set of scalar measures which decompose the conditional correlation, $R^2_{yx|z}$, summatively into three components: $R^2_{yx|z;-}$, $R^2_{yx|z;0}$ and $R^2_{yx|z;+}$ representing the components in the reverse, zero lag and forward directions, respectively. The estimated partial coherence, $|\hat{R}_{yx|z}(\lambda)|^2$ is decomposed summatively into three directional components: $|\hat{R}'_{yx|z;-}(\lambda)|^2$, $|\hat{R}'_{yx|z;0}(\lambda)|^2$ and $|\hat{R}'_{yx|z;+}(\lambda)|^2$. The framework includes complementary time and frequency domain measures. The time domain function, $\rho_{yx|z}(\tau)$, which is free from within variable effects, provides a direct indication of the directionality between processes (x, y) after removal of the common effects of process z.

Our framework has applicability to both time series and spike train data. As advances in multielectrode array recordings generate ever larger multivariate data sets with LFP and single unit recordings there is a need for appropriate signal processing tools to infer network dynamics. The novel non-parametric method presented here has the flexibility to combine spike train and time series data in a single framework, and is free from any concerns regarding the use of low order auto regressive models to represent electrophysiological signals. The framework should have broad application to a wide range of data including human electroencephalography (EEG) and magnetoencephalography (MEG).

5. Software

A software toolbox in MATLAB to undertake the analysis in this paper is available for free download. The software includes a user guide and example scripts. It is available from: http://www.neurospec.org/.

Acknowledgements

MHS is funded by The Ministry of Higher Education, Malaysia.

Appendix A. Algorithmic descriptions for two and three variable cases

This appendix includes algorithmic level descriptions of the two variable (Halliday, 2015), R^2_{yx}, and three variable, $R^2_{yx|z}$, analyses and their related quantities: directional metrics, frequency domain functions and time domain functions. The data vectors are assumed to have length R, where $R = LT$, the analysis uses only complete segments. The first step in both cases is the calculation of the discrete Fourier transform of the disjoint sections of length T over all L segments. This is indicated in line 3 of Algorithm 1 and line 3 of Algorithm 2 with the statement - Calculate: $d^T_x(\lambda, l)$, ... Summations are indicated using the notation sum$\{\cdot\}$, where necessary the range of the index is indicated after this, for example, all τ in line 16, or $\tau < 0$ in line 17 of Algorithm 1. Forward and inverse discrete Fourier transforms calculated with an fft algorithm are indicated using the notation fft$\{\cdot\}$ and ifft$\{\cdot\}$, respectively. Any reduced range in the independent variable is indicated using the same notation as the summation, for example, $\tau < 0$ in line 20 of Algorithm 1 indicates an FFT calculated using only negative values of τ, but using the same Fourier frequencies, all discrete Fourier transforms have length T, using zero padding where necessary. These algorithm descriptions follow the convention in MATLAB with respect to scaling factors in forward and reverse fft algorithms, namely a factor of T^{-1} is associated with the reverse transform, no scaling factor is included in the forward transform.

Algorithm 1. Unconditional directionality: R^2_{yx}

Input: x, y, T
Output: Metrics: $\hat{R}^2_{yx}, \hat{R}^2_{yx;-}, \hat{R}^2_{yx;0}, \hat{R}^2_{yx;+}$
Output: Frequency domain: $|\hat{R}_{yx}(\lambda)|^2, |\hat{R}'_{yx;-}(\lambda)|^2, |\hat{R}'_{yx;0}(\lambda)|^2, |\hat{R}'_{yx;+}(\lambda)|^2$
Output: Time domain: $\hat{\rho}_{yx}(\tau)$

1: $L \leftarrow R/T$
2: **for** $l = 1$ **to** L **do**
3: Calculate dFT: $d^T_x(\lambda, l), d^T_y(\lambda, l)$
4: **end for**
5: $\hat{f}_{xx}(\lambda) \leftarrow (2\pi LT)^{-1} \times \text{sum}\{|d^T_x(\lambda, l)|^2\}, l = 1, \ldots, L$
6: $\hat{f}_{yy}(\lambda) \leftarrow (2\pi LT)^{-1} \times \text{sum}\{|d^T_y(\lambda, l)|^2\}, l = 1, \ldots, L$
7: $\hat{w}_{xx}(\lambda) \leftarrow \hat{f}_{xx}(\lambda)^{-1/2}$
8: $\hat{w}_{yy}(\lambda) \leftarrow \hat{f}_{yy}(\lambda)^{-1/2}$
9: **for** $l = 1$ **to** L **do**
10: $dw^T_x(\lambda, l) \leftarrow d^T_x(\lambda, l) \times \hat{w}_{xx}(\lambda)$
11: $dw^T_y(\lambda, l) \leftarrow d^T_y(\lambda, l) \times \hat{w}_{yy}(\lambda)$
12: **end for**
13: $\hat{f}^w_{yx}(\lambda) \leftarrow (2\pi LT)^{-1} \times \text{sum}\{dw^T_y(\lambda, l) \times dw^{T^-}_x(\lambda, l)\}, l = 1, \ldots, L$
14: $|\hat{R}_{yx}(\lambda)|^2 \leftarrow |\hat{f}^w_{yx}(\lambda)|^2$
15: $\hat{\rho}_{yx}(\tau) \leftarrow \text{ifft}\{\hat{f}^w_{yx}(\lambda)\}$
16: $\hat{R}^2_{yx} \leftarrow \text{sum}\{\hat{\rho}_{yx}(\tau)^2\}$, all τ
17: $\hat{R}^2_{yx;-} \leftarrow \text{sum}\{\hat{\rho}_{yx}(\tau)^2\}, \tau < 0$
18: $\hat{R}^2_{yx;0} \leftarrow \{\hat{\rho}_{yx}(0)^2\}$
19: $\hat{R}^2_{yx;+} \leftarrow \text{sum}\{\hat{\rho}_{yx}(\tau)^2\}, \tau > 0$
20: $\hat{f}'_{yx;-}(\lambda) \leftarrow \text{fft}\{\hat{\rho}_{yx}(\tau)\}, \tau < 0$
21: $\hat{f}'_{yx;0}(\lambda) \leftarrow \hat{\rho}_{yx}(0)$
22: $\hat{f}'_{yx;+}(\lambda) \leftarrow \text{fft}\{\hat{\rho}_{yx}(\tau)\}, \tau > 0$
23: $S_{yx}(\lambda) \leftarrow |\hat{f}'_{yx;-}(\lambda)|^2 + |\hat{f}'_{yx;0}(\lambda)|^2 + |\hat{f}'_{yx;+}(\lambda)|^2$
24: $|\hat{R}'_{yx;-}(\lambda)|^2 \leftarrow (|\hat{f}'_{yx;-}(\lambda)|^2 / S_{yx}(\lambda)) \times |\hat{R}_{yx}(\lambda)|^2$
25: $|\hat{R}'_{yx;0}(\lambda)|^2 \leftarrow (|\hat{f}'_{yx;0}(\lambda)|^2 / S_{yx}(\lambda)) \times |\hat{R}_{yx}(\lambda)|^2$
26: $|\hat{R}'_{yx;+}(\lambda)|^2 \leftarrow (|\hat{f}'_{yx;+}(\lambda)|^2 / S_{yx}(\lambda)) \times |\hat{R}_{yx}(\lambda)|^2$

Algorithm 2. Conditional directionality: $R^2_{yx|z}$

Input: x, y, z, T
Output: Metrics: $\hat{R}^2_{yx|z}$, $\hat{R}^2_{yx|z;-}$, $\hat{R}^2_{yx|z;0}$, $\hat{R}^2_{yx|z;+}$
Output: Frequency domain: $|\hat{R}_{yx|z}(\lambda)|^2$, $|\hat{R}'_{yx|z;-}(\lambda)|^2$, $|\hat{R}'_{yx|z;0}(\lambda)|^2$, $|\hat{R}'_{yx|z;+}(\lambda)|^2$
Output: Time domain: $\hat{\rho}_{yx|z}(\tau)$

$L \leftarrow R/T$
for $l = 1$ **to** L **do**
  Calculate: $d^T_x(\lambda, l)$, $d^T_y(\lambda, l)$, $d^T_z(\lambda, l)$
end for
$\hat{f}_{zz}(\lambda) \leftarrow (2\pi LT)^{-1} \times \text{sum}\{|d^T_z(\lambda, l)|^2\}$, $l = 1, \ldots, L$
$\hat{f}_{xz}(\lambda) \leftarrow (2\pi LT)^{-1} \times \text{sum}\{d^T_x(\lambda, l) \times d^T_z(\bar{\lambda}, l)\}$, $l = 1, \ldots, L$
$\hat{f}_{yz}(\lambda) \leftarrow (2\pi LT)^{-1} \times \text{sum}\{d^T_y(\lambda, l) \times d^T_z(\bar{\lambda}, l)\}$, $l = 1, \ldots, L$
for $l = 1$ **to** L **do**
  $d^T_{x|z}(\lambda, l) \leftarrow d^T_x(\lambda, l) - (\hat{f}_{xz}(\lambda)/\hat{f}_{zz}(\lambda)) \times d^T_z(\lambda, l)$
  $d^T_{y|z}(\lambda, l) \leftarrow d^T_y(\lambda, l) - (\hat{f}_{yz}(\lambda)/\hat{f}_{zz}(\lambda)) \times d^T_z(\lambda, l)$
end for
$\hat{f}_{xx|z}(\lambda) \leftarrow (2\pi LT)^{-1} \times \text{sum}\{|d^T_{x|z}(\lambda, l)|^2\}$, $l = 1, \ldots, L$
$\hat{f}_{yy|z}(\lambda) \leftarrow (2\pi LT)^{-1} \times \text{sum}\{|d^T_{y|z}(\lambda, l)|^2\}$, $l = 1, \ldots, L$
$\hat{w}_{xx|z}(\lambda) \leftarrow \hat{f}_{xx|z}(\lambda)^{-1/2}$
$\hat{w}_{yy|z}(\lambda) \leftarrow \hat{f}_{yy|z}(\lambda)^{-1/2}$
for $l = 1$ **to** L **do**
  $dw^T_{x|z}(\lambda, l) \leftarrow d^T_{x|z}(\lambda, l) \times \hat{w}_{xx|z}(\lambda)$
  $dw^T_{y|z}(\lambda, l) \leftarrow d^T_{y|z}(\lambda, l) \times \hat{w}_{yy|z}(\lambda)$
end for
$\hat{f}^w_{yx|z}(\lambda) \leftarrow (2\pi LT)^{-1} \times \text{sum}\{dw^T_{y|z}(\lambda, l) \times dw^{T\,-}_{x|z}(\lambda, l)\}$, $l = 1, \ldots, L$
$|\hat{R}_{yx|z}(\lambda)|^2 \leftarrow |\hat{f}^w_{yx|z}(\lambda)|^2$
$\hat{\rho}_{yx|z}(\tau) \leftarrow \text{ifft}\{\hat{f}^w_{yx|z}(\lambda)\}$
$\hat{R}^2_{yx|z} \leftarrow \text{sum}\{\hat{\rho}_{yx|z}(\tau)^2\}$, all τ
$\hat{R}^2_{yx|z;-} \leftarrow \text{sum}\{\hat{\rho}_{yx|z}(\tau)^2\}$, $\tau < 0$
$\hat{R}^2_{yx|z;0} \leftarrow \{\hat{\rho}_{yx|z}(0)^2\}$
$\hat{R}^2_{yx|z;+} \leftarrow \text{sum}\{\hat{\rho}_{yx|z}(\tau)^2\}$, $\tau > 0$
$\hat{f}'_{yx|z;-}(\lambda) \leftarrow \text{fft}\{\hat{\rho}_{yx|z}(\tau)\}$, $\tau < 0$
$\hat{f}'_{yx|z;0}(\lambda) \leftarrow \hat{\rho}_{yx|z}(0)$
$\hat{f}'_{yx|z;+}(\lambda) \leftarrow \text{fft}\{\hat{\rho}_{yx|z}(\tau)\}$, $\tau > 0$
$S_{yx|z}(\lambda) \leftarrow |\hat{f}'_{yx|z;-}(\lambda)|^2 + |\hat{f}'_{yx|z;0}(\lambda)|^2 + |\hat{f}'_{yx|z;+}(\lambda)|^2$
$|\hat{R}'_{yx|z;-}(\lambda)|^2 \leftarrow (|\hat{f}'_{yx|z;-}(\lambda)|^2 / S_{yx|z}(\lambda)) \times |\hat{R}_{yx|z}(\lambda)|^2$
$|\hat{R}'_{yx|z;0}(\lambda)|^2 \leftarrow (|\hat{f}'_{yx|z;0}(\lambda)|^2 / S_{yx|z}(\lambda)) \times |\hat{R}_{yx|z}(\lambda)|^2$
$|\hat{R}'_{yx|z;+}(\lambda)|^2 \leftarrow (|\hat{f}'_{yx|z;+}(\lambda)|^2 / S_{yx|z}(\lambda)) \times |\hat{R}_{yx|z}(\lambda)|^2$

References

Baccala, L.A., Sameshima, K., 2001. Partial directed coherence: a new concept in neural structure determination. Biol. Cybern. 84, 463–474.
Brillinger, D.R., 1974. Fourier analysis of stationary processes. Proc. IEEE 62, 1628–1643.
Brillinger, D.R., 1975. Time Series – Data Analysis and Theory. Holt Rinehart & Winston Inc., New York.
Brillinger, D.R., 1988. Some statistical methods for random process data from seismology and neurophysiology. Ann. Stat. 16, 1–54.
Chen, Y., Bressler, S.L., Ding, M., 2006. Frequency decomposition of conditional Granger causality and application to multivariate neural field potential data. J. Neurosci. Methods 150, 228–237.
Chicharro, D., 2012. On the spectral formulation of Granger causality. Biol. Cybern. 105, 331–347.
Conway, B.A., Halliday, D.M., Rosenberg, J.R., 1993. Detection of weak synaptic interactions between single Ia-afferents and motor-unit spike trains in the decerebrate cat. J. Physiol. 471, 379–409.
Coomber, B., O'Donoghue, M.F., Mason, R., 2008. Inhibition of endocannabinoid metabolism attenuates enhanced hippocampal neuronal activity induced by kainic acid. Synapse 62, 746–755.
Destexhe, A., Rudolph, M., Pare, D., 2003. The high-conductance state of neocortical neurons in vivo. Nat. Rev. Neurosci. 4, 739–751.
Dhamala, M., Rangarajan, G., Ding, M., 2008a. Analyzing information flow in brain networks with nonparametric Granger causality. Neuroimage 41, 354–362.
Dhamala, M., Rangarajan, G., Ding, M., 2008b. Estimating Granger causality from fourier and wavelet transforms of time series data. Phys. Rev. Lett. 100, 18701.
Eichler, M., Dahlhaus, R., Sandkuhler, J., 2003. Partial correlation analysis for the identification of synaptic connections. Biol. Cybern. 89, 289–302.
Eldar, Y.C., Oppenheim, A.V., 2003. MMSE whitening and subspace whitening. IEEE Trans. Inf. Theory 49, 1846–1851.
Ezekiel, M., Fox, K.A., 1958. Methods of Correlation and Regression Analysis, 3rd ed. John Wiley, New York.
Gersch, W., 1972. Causality or driving in electrophysiological signal analysis. Math. Biosci. 14, 177–196.
Geweke, J.F., 1982. Measurement of linear dependence and feedback between multiple time series. J. Am. Stat. Assoc. 77, 304–324.
Geweke, J.F., 1984. Measures of conditional linear dependence and feedback between time series. J. Am. Stat. Assoc. 79, 907–915.
Granger, C.W.J., 1969. Investigating causal relations by econometric models and cross-spectral methods. Econometrica 37, 424–438.
Guo, S., Seth, A.K., Kendrick, K.M., Zhou, C., Feng, J., 2008. Partial Granger causality-eliminating exogenous inputs and latent variables. J. Neurosci. Methods 172 (1), 79–93.
Halliday, D.M., Rosenberg, J.R., Amjad, A.M., Breeze, P., Conway, B.A., Farmer, S.F., 1995. A framework for the analysis of mixed time series/point process data – theory and application to the study of physiological tremor, single motor unit discharges and electromyograms. Prog. Biophys. Mol. Biol. 64, 237–278.
Halliday, D.M., 2005. Spike-train analysis for neural systems. In: Reeke, G.N., Poznanski, R.R., Lindsay, K.A., Rosenberg, J.R., Sporns, O. (Eds.), Modeling in the Neurosciences, 2nd ed. Taylor & Francis, pp. 555–579.
Halliday, D.M., 2015. Non-parametric directionality measures for point process and time series data. J. Integr. Neurosci. 14 (2), 253–277.
Kaminski, M., Ding, M., Truccolo, W.A., Bressler, S.L., 2001. Evaluating causal relations in neural systems: Granger causality, directed transfer function and statistical assessment of significance. Biol. Cybern. 85, 145–157.
Lindsay, K.A., Rosenberg, J.R., 2011. Identification of directed interactions in networks. Biol. Cybern. 104, 385–396.
Medkour, T., Walden, A.T., Burgess, A., 2009. Graphical modelling for brain connectivity via partial coherence. J. Neurosci. Methods 180, 374–383.
Percival, D.B., Walden, A.T., 1993. Spectral Analysis for Physical Applications. Cambridge University Press, UK.
Pierce, D.A., 1979. R2 measures for time series. J. Am. Stat. Assoc. 74, 901–910.
Pierce, D.A., 1982. Comment on Geweke paper. J. Am. Stat. Assoc. 77, 315–316.
Priestley, M.B., 1981. Spectral Analysis and Time Series. Academic Press, London.
Rosenberg, J.R., Amjad, A., Breeze, P., Brillinger, D.R., Halliday, D.M., 1989. The Fourier approach to the identification of functional coupling between neuronal spike trains. Prog. Biophys. Mol. Biol. 53, 1–31.
Rosenberg, J.R., Halliday, D.M., Breeze, P., Conway, B.A., 1998. Identification of patterns of neuronal connectivity partial spectra, partial coherence and neuronal interactions. J. Neurosci. Methods 83, 57–72.
Rubinov, M., Sporns, O., 2010. Complex network measures of brain connectivity: uses and interpretations. Neuroimage 52, 1059–1069.
Salvador, R., Suckling, J., Schwarzbauer, C., Bullmore, E., 2005. Undirected graphs of frequency-dependent functional connectivity in whole brain networks. Philos. Trans. R. Soc. Lond. Ser. B: Biol. Sci. 360, 937–946.
Schelter, B., Winterhalder, M., Eichler, M., Peifer, M., Hellwig, B., Guschlbauer, B., Lucking, C.H., Dahlhaus, R., Timmer, J., 2006. Testing for directed influences among neural signals using partial directed coherence. J. Neurosci. Methods 152, 210–219.
Senik, M.H., O'Donoghue, M.F., Mason, R.,2013. Intra- and inter-hippocampal connectivity in a KA-induced mTLE rat model. Program No. 143.05. In: 2013 Neuroscience Meeting Planner. Society for Neuroscience, San Diego, CA, Online.
Thomson, D.J., Chave, A., 1991. Jackknifed error estimates for spectra, coherences, and transfer functions. In: Haykin, S. (Ed.), In: Advances in Spectrum Analysis and Array Processing, vol. 1, pp. 58–113.
Tick, L.J., 1963. Conditional spectra, linear systems and coherency. In: Rosenblatt, M. (Ed.), Time Series Analysis. Wiley, New York, pp. 197–203.
Troyer, T.W., Miller, K.D., 1997. Physiological gain leads to high ISI variability in a simple model of a cortical regular spiking cell. Neural Comput. 9, 971–983.